

Unconventional Vortices and Phase Transitions in Rapidly Rotating Superfluid ^3He

Takafumi Kita*

Division of Physics, Hokkaido University, Sapporo 060-0810, Japan

(Dated: November 9, 2018)

This paper studies vortex-lattice phases of rapidly rotating superfluid ^3He based on the Ginzburg-Landau free-energy functional. To identify stable phases in the p - Ω plane (p : pressure; Ω : angular velocity), the functional is minimized with the Landau-level expansion method using up to 3000 Landau levels. This system can sustain various exotic vortices by either (i) shifting vortex cores among different components or (ii) filling in cores with components not used in the bulk. In addition, the phase near the upper critical angular velocity Ω_{c2} is neither the A nor B phases, but the polar state with the smallest superfluid density, as already shown by Schopohl. Thus, multiple phases are anticipated to exist in the p - Ω plane. Six different phases are found in the present calculation performed over $0.0001\Omega_{c2} \leq \Omega \leq \Omega_{c2}$, where Ω_{c2} is of order $(1-T/T_c) \times 10^7$ rad/s. It is shown that the double-core vortex experimentally found in the B phase originates from the polar hexagonal lattice near Ω_{c2} via (i) a phase composed of interpenetrating polar and Scharnberg-Klemm sublattices; (ii) the A-phase mixed-twist lattice with polar cores; (iii) the normal-core lattice found in the isolated-vortex calculation by Ohmi, Tsuneto, and Fujita; and (iv) the A-phase-core vortex discovered in another isolated-vortex calculation by Salomaa and Volovik. It is predicted that the double-core vortex will disappear completely in the experimental p - T phase diagram to be replaced by the A-phase-core vortex for $\Omega \gtrsim 10^3 \sim 10^4$ rad/s. C programs to minimize a single-component Ginzburg-Landau functional are available at <http://phys.sci.hokudai.ac.jp/~kita/index-e.html>.

PACS numbers: 67.57.Fg, 74.60.-w

I. INTRODUCTION

Rotating superfluid ^3He with 9 complex order parameters can sustain various exotic vortices not observable in superfluid ^4He . This system can be a text-book case of unconventional vortices realized in multi-component superfluids and superconductors. I here report the richness and diversity of the vortex phase diagram in the unexplored region of rapid rotation, wishing to stimulate experiments in the frontiers as well as to give hints to what may be expected in the vortex phases of multi-component superconductors.

Extensive efforts have been made both theoretically and experimentally to clarify vortices of superfluid ^3He ; see Refs. 1–7 for a review. With multi-component order parameters, this system can be a rich source of unconventional vortices. Those already observed in rotation up to 3 rad/s include: superfluid-core vortices in the B phase, i.e., the A-phase-core and double-core vortices;^{8–11} vortices due to textures of the \mathbf{l} -vector in the A phase, i.e., the locked vortex^{1,12,13} the continuous unlocked vortex,^{14,15} the singular vortex,^{15,16} and the vortex sheet.¹⁷ The superfluid cores are possible in the B phase because the components not used in the bulk are available to fill in them. On the other hand, the A phase has a unique property that it can sustain vortices by a spatial variation of \mathbf{l} without any amplitude reduction, as first pointed out by Mermin and Ho.¹⁸ Thus, experiments have already revealed rich structures.

Although $\Omega \sim 3$ rad/s is three orders of magnitude faster than the lower critical angular velocity $\Omega_{c1} \sim 10^{-3}$ rad/s for a typical experimental cell of diameter ~ 5 mm, it is still far below the upper critical angular velocity

$\Omega_{c2} \sim (1-T/T_c) \times 10^7$ rad/s. Thus, theoretical calculations have been performed mostly within the isolated-vortex approximation in the B phase,^{10,11,19,20} or within a constant amplitude in the A phase,^{12,15,17,21,22} both of which are justified near Ω_{c1} , and not much has been known about the phases realized in rapid rotation. On the other hand, the polar state should be stable near Ω_{c2} at all pressures, as shown by Schopohl²³ and later by Scharnberg and Klemm²⁴ in a different context of p -wave superconductivity. This is because the line node of the polar state is most effective in reducing the kinetic energy dominant near Ω_{c2} . Thus, the phase near Ω_{c2} is completely different from the experimentally observed A and B phases at $\Omega=0$, and there should be novel phases between Ω_{c1} and Ω_{c2} . Although $\Omega_{c2} \sim (1-T/T_c) \times 10^7$ rad/s may not be attainable in the near future, clarifying the whole phase diagram of $\Omega_{c1} \leq \Omega \leq \Omega_{c2}$ would stimulate experimental efforts towards the direction; it certainly remains as an intellectual challenge. In addition, such a study will be useful in providing an insight into the vortices of multi-component superconductors where H_{c2} can be reached easily.

Following a previous work,²⁵ I present a more extensive study on vortices in superfluid ^3He . To this end, I adopt the standard Ginzburg-Landau (GL) free-energy functional valid near T_c , as most calculations performed so far. To clarify the vortex phase diagram, however, I take an alternative approach to start from Ω_{c2} proceeding down towards Ω_{c1} as close as possible. A powerful way to carry out this program is the Landau-level expansion method (LLX), developed recently^{26,27} and applied successfully to several other systems.^{28–30} Combining the obtained results with those around Ω_{c1} will provide a rough idea about the whole phase diagram over

$\Omega_{c1} \leq \Omega \leq \Omega_{c2}$. It should also be noted that the results from the GL functional are expected to provide qualitatively correct results over $0 \leq T \leq T_c$, as supported by a recent isolated-vortex calculation on the B phase²⁰ using the quasiclassical theory.³¹

This paper is organized as follows. Section II presents the GL functional. Section III explains LLX to minimize the GL functional. Section IV provides a group-theoretical consideration on the classification of vortex lattices and the phase transitions between them. Section V presents the obtained p - Ω phase diagram over $0.01\Omega_{c2} \leq \Omega \leq \Omega_{c2}$ together with detailed explanations on the phases appearing in it. Section VI discusses a phase transition between the A-phase-core and double-core lattices extending the calculation down to $0.0001\Omega_{c2}$. Section VII summarizes the paper. Appendix A presents basic properties of the basis functions used in LLX.

II. GINZBURG-LANDAU FUNCTIONAL

Superfluid ³He is characterized by 9 complex order parameters $A_{\mu i}$ ($\mu, i = x, y, z$) inherent in the p -wave pairing ($L=1$) with spin $S=1$, where μ and i denotes rectangular coordinates of the spin and orbital spaces, respectively. The GL free-energy functional near T_c is given with respect to the second- and fourth-order terms of $A_{\mu i}$. Using the notation of Fetter,¹ the bulk energy density reads

$$\begin{aligned} f_b = & -\alpha A_{\mu i}^* A_{\mu i} + \beta_1 A_{\mu i}^* A_{\mu i} A_{\nu j} A_{\nu j} + \beta_2 A_{\mu i}^* A_{\nu j}^* A_{\mu i} A_{\nu j} \\ & + \beta_3 A_{\mu i}^* A_{\nu i}^* A_{\mu j} A_{\nu j} + \beta_4 A_{\mu i}^* A_{\nu j}^* A_{\mu j} A_{\nu i} \\ & + \beta_5 A_{\mu i}^* A_{\mu j}^* A_{\nu i} A_{\nu j}, \end{aligned} \quad (1)$$

where α and β_j are coefficients, and summations over repeated indices are implied. The gradient energy density is well approximated using a single coefficient K as

$$f_k = K(\partial_i^* A_{\mu i}^* \partial_j A_{\mu j} + \partial_i^* A_{\mu j}^* \partial_i A_{\mu j} + \partial_i^* A_{\mu j}^* \partial_j A_{\mu i}), \quad (2)$$

where ∂ is defined in terms of the angular velocity Ω as

$$\partial \equiv \nabla - i \frac{2m_3}{\hbar} \Omega \times \mathbf{r}. \quad (3)$$

In addition, there are tiny contributions from the dipole and Zeeman energies:

$$f_d = g_d (A_{\mu\mu}^* A_{\nu\nu} + A_{\mu\nu}^* A_{\nu\mu} - \frac{2}{3} A_{\mu\nu}^* A_{\mu\nu}), \quad (4)$$

$$f_m = g_m H_\mu A_{\mu i}^* H_\nu A_{\nu i}, \quad (5)$$

respectively. Given the coefficients in Eqs. (1)-(5), the stable state can be found by minimizing

$$F = F_0 + F_1 \quad (6)$$

with

$$F_0 \equiv \frac{1}{V} \int (f_b + f_k) d\mathbf{r}, \quad (7a)$$

$$F_1 \equiv \frac{1}{V} \int (f_d + f_m) d\mathbf{r}, \quad (7b)$$

where V is the volume of the system. Important quantities in the functional are

$$\xi \equiv (K/\alpha)^{1/2} = \xi(0)/(1-T/T_c)^{1/2}, \quad (8a)$$

$$\xi_d \equiv (K/g_d)^{1/2}, \quad (8b)$$

$$H_d \equiv (g_d/g_m)^{1/2}, \quad (8c)$$

which define the GL coherence length, the dipole length, and the characteristic magnetic dipole field, respectively.

The coefficients α , β_j , K , g_m , and g_d are fixed by exactly following Thuneberg's procedure¹¹ used in identifying the B-phase core structures as follows. The weak-coupling theory yields¹

$$\alpha = \frac{N(0)}{3} (1-T/T_c), \quad (9a)$$

$$\beta_2^W = \beta_3^W = \beta_4^W = -\beta_5^W = -2\beta_1^W = \frac{7\zeta(3)N(0)}{120(\pi k_B T_c)^2}, \quad (9b)$$

$$K = \frac{7\zeta(3)N(0)(\hbar v_F)^2}{240(\pi k_B T_c)^2}, \quad (9c)$$

where $N(0)$ and v_F are the density of states per spin and the Fermi velocity, respectively. The coefficients α and K are estimated by Eqs. (9b) and (9c) using the values of $N(0)$, T_c , and v_F determined experimentally by Greywall.³² In contrast, β_j^W cannot account for the stability of the A phase at $\Omega = 0$. Strong-coupling corrections are included in β_j by (i) using the Sauls-Serene values for $1.2 \text{ MPa} \leq p \leq 3.44 \text{ MPa}$;³³ (ii) adopting the weak-coupling result β_j^W at $p = 0 \text{ MPa}$; and (iii) interpolating the region $0 \text{ MPa} \leq p \leq 1.2 \text{ MPa}$. With this procedure, the A-B transition for $\Omega = 0$ is predicted at

$$p_{\text{pcp}} = 2.85 \text{ MPa}. \quad (10)$$

It thus yields a qualitatively correct result that the A phase is stabilized on the high-pressure side, although the value is slightly higher than the measured 2.1 MPa. The values of g_d have been studied extensively in a recent paper by Thuneberg.³⁴ It is shown that the following formula nicely reproduces the values extracted from various experiments:

$$g_d = \frac{\mu_0}{40} \left[\gamma \hbar N(0) \ln \frac{1.1339 \times 0.45 T_F}{T_c} \right]^2, \quad (11a)$$

where μ_0 and γ denotes the permeability of vacuum and the gyromagnetic ratio, respectively, and T_F is the Fermi temperature defined by $T_F \equiv 3n/4N(0)k_B$ with n denoting the density. As for g_m , the following weak-coupling expression is sufficient:

$$g_m = \frac{7\zeta(3)N(0)(\gamma\hbar)^2}{48[(1+F_0^a)\pi k_B T_c]^2}, \quad (11b)$$

with F_0^a the Landau parameter. The values of F_0^a are taken from Wheatley³⁵ but corrected for the newly determined F_1^s by Greywall;³² this $F_1^s(p)$ is tabulated conveniently in Ref. 4. Table I summarizes the pressure dependences of basic quantities thus calculated.

TABLE I: Numerical values for the parameters of the GL theory at different pressures. See text for details of the calculations.

p [10^6 Pa]	$\alpha/(1-T/T_c)$ [10^{50} J $^{-1}$ m $^{-3}$]	β_3 [10^{99} J $^{-3}$ m $^{-3}$]	K [10^{34} J $^{-1}$ m $^{-1}$]	$\xi(1-T/T_c)^{1/2}$ [10^{-8} m]	ξ_d [10^{-5} m]	H_d [10^{-3} T]	$\Omega_{c2}/(1-T/T_c)$ [10^6 rad/s]
0.0	1.68	21.7	41.8	5.00	4.91	0.803	2.10
0.4	2.03	11.5	17.8	2.96	2.85	1.09	5.98
0.8	2.33	8.55	11.2	2.19	2.05	1.32	10.9
1.2	2.59	7.29	8.32	1.79	1.64	1.48	16.4
1.6	2.85	6.71	6.71	1.54	1.38	1.60	22.3
2.0	3.09	6.43	5.70	1.36	1.19	1.73	28.5
2.4	3.33	6.33	5.02	1.23	1.05	1.85	34.9
2.8	3.57	6.39	4.54	1.13	0.949	1.96	41.3
3.2	3.81	6.56	4.19	1.05	0.864	2.04	47.8
3.44	3.96	6.69	4.02	1.01	0.821	2.10	51.7

It should be noted finally that, although Thuneberg's procedure is adopted here, qualitative features of the phase diagram (Fig. 1) obtained below are expected to be the same among the models for $\beta_j = \beta_j(p)$ which yields the A-B transition at $\Omega = 0$. This has been checked for the spin-fluctuation-feedback model of Anderson and Brinkman.^{36,37}

III. METHOD

To minimize Eq. (6), let us first rewrite the order parameters as

$$A_{\mu i} = R_{\mu\nu} \tilde{A}_{\nu i}, \quad (12)$$

where $R_{\mu\nu}$ denotes the spin-space rotation and $\tilde{A}_{\nu i}$ is the order parameter of the restricted space where the spin coordinates are fixed conveniently relative to the orbital ones. We then find that the gradients of $\tilde{A}_{\nu i}$ and $R_{\mu\nu}$ do not couple in Eq. (2) due to the orthogonormality: $R_{\mu\lambda} R_{\nu\lambda} = \delta_{\mu\nu}$. The characteristic lengths for $\tilde{A}_{\nu i}$ and $R_{\mu\nu}$ are given by ξ and ξ_d of Table I, respectively, where we observe that ξ_d is much longer than both ξ and the intervortex distance l_c defined below in Eq. (14) for the relevant range $0.0001\Omega_{c2} \leq \Omega \leq \Omega_{c2}$ considered here. It hence follows that $R_{\mu\nu}$ is virtually kept constant in space. It can be fixed by Eq. (7b) after obtaining $\tilde{A}_{\nu i}$ from Eq. (7a). This is due to the smallness of Eq. (7b) relative to Eq. (7a).

To minimize Eq. (7a) with respect to $\tilde{A}_{\nu i}$, I assume uniformity along $\Omega \parallel \hat{\mathbf{z}}$. I then define creation and annihilation operators (a^\dagger, a) satisfying $aa^\dagger - a^\dagger a = 1$ as

$$a^\dagger \equiv \frac{l_c}{\sqrt{2}}(-\partial_x + i\partial_y), \quad a \equiv \frac{l_c}{\sqrt{2}}(\partial_x + i\partial_y), \quad (13)$$

with

$$l_c \equiv (\hbar/4m_3\Omega)^{1/2}. \quad (14)$$

It is also convenient to introduce the quantities:

$$\tilde{A}_\mu^{(0)} \equiv \tilde{A}_{\mu z}, \quad \tilde{A}_\mu^{(\pm 1)} \equiv \frac{1}{\sqrt{2}}(\tilde{A}_{\mu x} \mp i\tilde{A}_{\mu y}), \quad (15)$$

which denote the expansion coefficients of \hat{k}_z and $(\hat{k}_x \pm i\hat{k}_y)/\sqrt{2}$, respectively. Now, Eq. (2) can be rewritten in terms of Eqs. (13)-(15) as

$$f_k = \frac{K}{l_c^2} \left\{ (1+|m|) [\tilde{A}_\mu^{(m)*} \tilde{A}_\mu^{(m)} + 2(a\tilde{A}_\mu^{(m)})^* a\tilde{A}_\mu^{(m)}] \right. \\ \left. - 2[(a\tilde{A}_\mu^{(1)})^* a^\dagger \tilde{A}_\mu^{(-1)} + a\tilde{A}_\mu^{(1)}(a^\dagger \tilde{A}_\mu^{(-1)})^*] \right\}. \quad (16)$$

Equations (1), (4), and (5) are transformed similarly using $A_{\mu i}^* A_{\nu i} = A_\mu^{(m)*} A_\nu^{(m)}$ and $A_{\mu i} A_{\nu i} = A_\mu^{(m)} A_\nu^{(-m)}$.

From Eq. (16) and the bilinear term in Eq. (1), we find that the p -wave superfluid transition is split, due to the uniaxial anisotropy Ω , essentially into those of different m channels as

$$\left\{ \begin{array}{ll} \Omega_{c2}^{(0)} = \frac{\hbar\alpha}{4m_3K} \equiv \Omega_{c2} & : \text{polar} \\ \Omega_{c2}^{(-1)} = \frac{3+\sqrt{6}}{6}\Omega_{c2} & : \text{ABM}^-(\text{SK}) \\ \Omega_{c2}^{(1)} = \frac{1}{2}\Omega_{c2} & : \text{ABM}^+ \end{array} \right. , \quad (17)$$

in agreement with the results of Schopohl²³ and Scharnberg and Klemm.²⁴ Here the first and third ones correspond to the polar state ($\propto \hat{k}_z$) and the Anderson-Brinkman-Morel (ABM) state ($\propto \hat{k}_x + i\hat{k}_y$) with $l_z = 1$, respectively, both in the $N = 0$ Landau level. In contrast, the ABM^- (also called as Scharnberg-Klemm or SK state) is not a pure ABM state; it is made up of the $\hat{k}_x - i\hat{k}_y$ state in the $N = 0$ Landau level and the $\hat{k}_x + i\hat{k}_y$ state in the $N = 2$ Landau level. Equation (17) tells us that it is the polar state $\tilde{A}_\mu^{(0)} \neq 0$ which is realized at Ω_{c2} . Its stability is due to the line node in the xy plane perpendicular to Ω which works favorably to reduce the kinetic energy dominant near Ω_{c2} . Indeed, given the condition that the average gap amplitude on the Fermi surface is constant, the superfluid density ρ_{xx} of the polar state $\rho_{xx}^{\text{polar}} \propto 3 \int d\Omega_{\mathbf{k}} \hat{k}_x^2 \hat{k}_z^2 = 3/15$ is half that of the ABM state $\rho_{xx}^{\text{ABM}} \propto \frac{3}{2} \int d\Omega_{\mathbf{k}} \hat{k}_x^2 (\hat{k}_x^2 + \hat{k}_y^2) = 6/15$. This explains the difference of the factor 2 between $\Omega_{c2} = \Omega_{c2}^{(0)}$ and $\Omega_{c2}^{(1)}$. As seen in Table I, this Ω_{c2} is of order $(1-T/T_c) \times 10^7$ rad/s.

With these preparations, Eq. (7a) is minimized by LLX.²⁶ In the end, it can be performed quite efficiently, especially near Ω_{c2} , with the Ritz variational method of expanding $\tilde{A}_\mu^{(m)}$ in some basis functions and carrying out the minimization with respect to the expansion coefficients. Convenient basis functions for periodic vortex lattices are obtained using the magnetic translation operator:

$$T_{\mathbf{R}} \equiv \exp[-\mathbf{R} \cdot (\nabla + 2im_3\mathbf{\Omega} \times \mathbf{r}/\hbar)], \quad (18)$$

where \mathbf{R} denotes a lattice point spanned by two basic vectors:

$$\begin{cases} \mathbf{a}_1 \equiv (a_{1x}, a_{1y}, 0) \\ \mathbf{a}_2 \equiv (0, a_2, 0) \end{cases}, \quad a_{1x}a_2 = 2\pi l_c^2. \quad (19)$$

Hence those lattices have a unit circulation quantum $\kappa \equiv h/2m_3$ per every basic cell,¹ as required. The basic vectors of the corresponding reciprocal lattice are given by

$$\begin{cases} \mathbf{b}_1 \equiv (\mathbf{a}_2 \times \hat{\mathbf{z}})/l_c^2 \\ \mathbf{b}_2 \equiv (\hat{\mathbf{z}} \times \mathbf{a}_1)/l_c^2 \end{cases}. \quad (20)$$

The magnetic Bloch vector is defined in the Brillouin zone of the reciprocal lattice as

$$\mathbf{q} \equiv \frac{\mu_1}{\mathcal{N}_f} \mathbf{b}_1 + \frac{\mu_2}{\mathcal{N}_f} \mathbf{b}_2 \quad \left(-\frac{\mathcal{N}_f}{2} < \mu_j \leq \frac{\mathcal{N}_f}{2} \right), \quad (21)$$

where \mathcal{N}_f is an even integer with \mathcal{N}_f^2 denoting the number of κ in the system. Using these quantities, the basis functions are obtained as simultaneous eigenstates of $a^\dagger a$ and $T_{\mathbf{R}}$ as²⁶

$$\begin{aligned} \psi_{N\mathbf{q}}(\mathbf{r}) = & \sum_{n=-\mathcal{N}_f/2+1}^{\mathcal{N}_f/2} e^{i[q_y(y+l_c^2 q_x/2) + na_{1x}(y+l_c^2 q_x - na_{1y}/2)/l_c^2]} \\ & \times e^{-ixy/2l_c^2 - (x-l_c^2 q_y - na_{1x})^2/2l_c^2} \\ & \times \sqrt{\frac{2\pi l_c/a_2}{2^N N! \sqrt{\pi} V}} H_N\left(\frac{x-l_c^2 q_y - na_{1x}}{l_c}\right), \quad (22) \end{aligned}$$

where N denotes the Landau level and H_N is the Hermite polynomial.³⁸ Useful properties of $\psi_{N\mathbf{q}}$ are summarized in Appendix A. Let us expand $\tilde{A}_\mu^{(m)}$ in $\{\psi_{N\mathbf{q}}\}$ as

$$\tilde{A}_\mu^{(m)}(\mathbf{r}) = \sqrt{V} \sum_{N=0}^{\infty} \sum_{\mathbf{q}} c_{N\mathbf{q}}^{(\mu m)} \psi_{N\mathbf{q}}(\mathbf{r}). \quad (23)$$

Then substitute Eq. (23) into Eq. (7a), perform a change of variables $(x, y) = (a_{1x}s, a_{1y}s + a_2t)$, and carry out the integration in Eq. (7a) with respect to (s, t) . Now, Eq. (7a) is transformed into a functional of the expansion coefficients $\{c_{N\mathbf{q}}^{(\mu m)}\}$ and a couple of lattice parameters:

$$\begin{cases} \beta \equiv \cos^{-1}(a_{1y}/a_1) & : \text{apex angle} \\ \rho \equiv a_2/a_1 & : \text{length ratio} \end{cases}, \quad (24)$$

as

$$F_0 = F_0[\{c_{N\mathbf{q}}^{(\mu m)}\}, \beta, \rho]. \quad (25)$$

For a given Ω , this F_0 is minimized directly.

Numerical minimizations have been performed as follows: (i) Cut the series in Eq. (23) at some N_{\max} and substitute it into Eq. (7a). The convergence can be checked by increasing N_{\max} , as increasing N_{\max} is guaranteed to yield a better solution with a lower F_0 . (ii) Numerical integrations in Eq. (7a) are performed using the trapezoidal rule which is known very powerful for periodic functions. To this end, the basis functions of $N \leq N_{\max}$ on the discrete points are tabulated at the beginning of the calculations. Equation (25) is thereby evaluated for each set of arguments. It has been necessary to increase N_{\max} from 6 near Ω_{c2} to 360 at $0.01\Omega_{c2}$, and the integration points in the basic cell from 6^2 to 36^2 accordingly to obtain the relative accuracy of order 10^{-8} for F_0 . (iii) Equation (25) is minimized first with respect to $\{c_{N\mathbf{q}}^{(\mu m)}\}$ by Powell's method or the conjugate gradient method,³⁹ and then, if necessary, with respect to (β, ρ) by Powell's method. The conjugate gradient method is about 10 times faster, although the programming is far more cumbersome. Powell's method is fast enough for $\Omega \gtrsim 0.05\Omega_{c2}$. (iv) Second-order transitions are identified carefully by combining group-theoretical considerations of Sec. IV with signals of the relative change in the slope of $\partial F_0/\partial\Omega$. Its analytic expression is obtained as^{26,40}

$$\frac{\partial F_0}{\partial\Omega} = \frac{1}{\Omega} \int f_{\mathbf{k}} \, d\mathbf{r}, \quad (26)$$

so that it can be calculated quite accurately without recourse to any numerical differentiation.

Once $\tilde{A}_{\mu i}$ are fixed as above, Eq. (12) is substituted into Eq. (7b). Considering $R_{\mu\nu}$ constant in space, as mentioned before, the three independent parameters of the matrix \underline{R} are then determined by minimizing Eq. (7b).

Some phases encountered below have a common feature that all the components other than

$$\mathbf{d} \equiv (R_{xz}, R_{yz}, R_{zz}); \quad \tilde{\mathbf{A}} \equiv (\tilde{A}_{zx}, \tilde{A}_{zy}, \tilde{A}_{zz}) \quad (27)$$

can be put equal to zero. For those states, F_1 is given by

$$F_1 = g_d(\hat{d}_\mu M_{\mu\nu} \hat{d}_\nu - \frac{2}{3}(\tilde{\mathbf{A}}^* \cdot \tilde{\mathbf{A}})), \quad (28)$$

where $\langle \dots \rangle \equiv \frac{1}{V} \int \dots d\mathbf{r}$, and $M_{\mu\nu}$ is defined by

$$M_{\mu\nu} \equiv \langle 2\tilde{A}_\mu^* \tilde{A}_\nu + \tilde{\mathbf{A}}^* \cdot \tilde{\mathbf{A}} H_\mu H_\nu / H_d^2 \rangle. \quad (29)$$

It hence follows that \mathbf{d} points parallel to the eigenvector corresponding to the smallest eigenvalue of \underline{M} .

IV. GROUP-THEORETICAL CONSIDERATIONS

A. Classification of Vortices

As in the case of ordinary solids,^{41,42} various vortex lattices can be classified according to their symmetry. It turns out that the operator (18), the basis functions (22), and the expansion (23) are quite useful for this purpose.

Classification of isolated vortices in superfluid ³He has been carried out by Salomaa and Volovik^{2,10} and Thuneberg.¹¹ Such classification for vortex lattices has been performed recently by Karimäki and Thuneberg,²² without recourse to Eqs. (18)-(23), however. It is shown below that making use of Eqs. (18)-(23) provides a transparent classification scheme.

To start with it is necessary to define ‘‘symmetry operations’’ unambiguously, since we are considering a phenomenological GL functional rather than a microscopic Hamiltonian. In the case of a Hamiltonian, ‘‘symmetry operations’’ mean those operations which commute with the Hamiltonian. In the present case of a GL functional, ‘‘symmetry operations’’ are defined as those operations which keep all the physical (i.e. observable) quantities invariant. Let us restrict ourselves to orbital degrees of freedom, as appropriate when Eq. (7b) can be regarded as a tiny perturbation. Then, besides $f_b + f_k$ of Eqs. (1) and (2), there are three relevant physical quantities:

$$\rho(\mathbf{r}) \equiv \tilde{A}_{\mu i}^* \tilde{A}_{\mu i}, \quad (30a)$$

$$j_i(\mathbf{r}) \equiv \frac{4m_3 K}{\hbar} \text{Im}(\tilde{A}_{\mu i}^* \partial_j \tilde{A}_{\mu j} + \tilde{A}_{\mu j}^* \partial_i \tilde{A}_{\mu j} + \tilde{A}_{\mu j}^* \partial_j \tilde{A}_{\mu i}), \quad (30b)$$

$$l_i(\mathbf{r}) \equiv -i\varepsilon_{ijk} \tilde{A}_{\mu j}^* \tilde{A}_{\mu k} / \rho(\mathbf{r}), \quad (30c)$$

which denote the density, current, and normalized orbital angular momentum of Cooper pairs, respectively. A general operator $\hat{\mathcal{S}}$ transforms $\tilde{A}_{\mu i}$, ∂_i , and ε_{ijk} in these expressions as

$$\tilde{A}_{\mu i}(\mathbf{r}) \rightarrow \tilde{A}_{\mu i}^{(\mathcal{S})}(\mathbf{r}) \equiv \mathcal{S}_{\mu\nu} \tilde{A}_{\nu j}(\underline{\mathcal{S}}^{-1}\mathbf{r}) \mathcal{S}_{ji}^{-1}, \quad (31a)$$

$$\partial_i \rightarrow \partial_i^{(\mathcal{S})} \equiv \mathcal{S}_{ii'} \partial_{i'}, \quad (31b)$$

$$\varepsilon_{ijk} \rightarrow \varepsilon_{ijk}^{(\mathcal{S})} \equiv \mathcal{S}_{ii'} \mathcal{S}_{jj'} \mathcal{S}_{kk'} \varepsilon_{i'j'k'}, \quad (31c)$$

where $(\underline{\mathcal{S}})_{\mu\nu} = \mathcal{S}_{\mu\nu}$ denotes a matrix representation of $\hat{\mathcal{S}}$. Now, symmetry of a vortex lattice is specified by those operations $\{\hat{\mathcal{S}}\}$ which keep the physical quantities invariant as

$$\begin{cases} f_b(\mathbf{r}) + f_k(\mathbf{r}) = f_b^{(\mathcal{S})}(\mathbf{r}) + f_k^{(\mathcal{S})}(\mathbf{r}) \\ \rho(\mathbf{r}) = \rho^{(\mathcal{S})}(\mathbf{r}) \\ \mathbf{j}(\mathbf{r}) = \mathbf{j}^{(\mathcal{S})}(\mathbf{r}) \\ \mathbf{l}(\mathbf{r}) = \mathbf{l}^{(\mathcal{S})}(\mathbf{r}) \end{cases}, \quad (32)$$

where $\mathbf{j}^{(\mathcal{S})}$, for example, denotes the expression obtained by substituting Eq. (31) into Eq. (30b). The collection of

these operations $\{\hat{\mathcal{S}}\}$ forms a group, which characterize the relevant vortex lattice.

Since $T_{\mathbf{R}}$ of Eq. (18) commutes with $\hat{\mathcal{D}}$ of Eq. (3), the operator $T_{\mathbf{R}}$ plays exactly the same role as the translation operator of the ordinary space group. This is one of the main reasons why the basis functions (22), which are eigenstates of $T_{\mathbf{R}}$, is advantageous in expanding the order parameters as Eq. (23).

As an example, let us specifically consider Phase IV of Fig. 1 given below. It corresponds to the hexagonal lattice of the normal-core vortex in the B phase which was discovered in the isolated-vortex calculation by Ohmi, Tsuneto, and Fujita.¹⁹ The present calculation with LLX shows that non-zero order parameters can be expressed as

$$\tilde{A}_z^{(0)} = \sqrt{V} \sum_N c_{N\mathbf{q}_1}^{(0)} \psi_{N\mathbf{q}_1}, \quad (33a)$$

$$\tilde{A}_x^{(-1)} = \sqrt{V} \sum_N [c_{N\mathbf{q}_1}^{(-1)} \psi_{N\mathbf{q}_1} + c_{N+4\mathbf{q}_1}^{(-1)} \psi_{N+4\mathbf{q}_1}], \quad (33b)$$

$$\tilde{A}_y^{(-1)} = i\sqrt{V} \sum_N [c_{N\mathbf{q}_1}^{(-1)} \psi_{N\mathbf{q}_1} - c_{N+4\mathbf{q}_1}^{(-1)} \psi_{N+4\mathbf{q}_1}], \quad (33c)$$

$$\tilde{A}_x^{(1)} = \sqrt{V} \sum_N [c_{N\mathbf{q}_1}^{(1)} \psi_{N\mathbf{q}_1} + c_{N+2\mathbf{q}_1}^{(1)} \psi_{N+2\mathbf{q}_1}], \quad (33d)$$

$$\tilde{A}_y^{(1)} = -i\sqrt{V} \sum_N [c_{N\mathbf{q}_1}^{(1)} \psi_{N\mathbf{q}_1} - c_{N+2\mathbf{q}_1}^{(1)} \psi_{N+2\mathbf{q}_1}], \quad (33e)$$

where the summations run over $N=6n$ ($n=0, 1, 2, \dots$), \mathbf{q}_1 is a magnetic Bloch vector which can be chosen arbitrarily due to the broken translational symmetry, and all $c_{N\mathbf{q}_1}^{(m)}$'s are real. It is convenient to fix $\mathbf{q}_1 = \frac{1}{2}(\mathbf{b}_1 + \mathbf{b}_2)$ so that a core is located at the origin, i.e., $\tilde{A}_i^{(m)}(\mathbf{0}) = 0$. Then, with the properties of $\psi_{N\mathbf{q}_1}$ given by Eq. (A8), one can show that the order-parameter matrix $(\tilde{A})_{\mu i} \equiv \tilde{A}_{\mu i}$ satisfies

$$\underline{R}_\varphi \tilde{A} (\underline{R}_\varphi^{-1}\mathbf{r}) \underline{R}_\varphi^{-1} = e^{-i\varphi} \tilde{A}(\mathbf{r}), \quad (34a)$$

$$\underline{\sigma}_x \tilde{A}^* (\underline{\sigma}_x^{-1}\mathbf{r}) \underline{\sigma}_x^{-1} = e^{-5i\pi/4} \tilde{A}(\mathbf{r}), \quad (34b)$$

$$\underline{\sigma}_y \tilde{A}^* (\underline{\sigma}_y^{-1}\mathbf{r}) \underline{\sigma}_y^{-1} = e^{-i\pi/4} \tilde{A}(\mathbf{r}), \quad (34c)$$

$$\underline{\sigma}_h \tilde{A} (\underline{\sigma}_h^{-1}\mathbf{r}) \underline{\sigma}_h^{-1} = \tilde{A}(\mathbf{r}), \quad (34d)$$

where \underline{R}_φ and $\underline{\sigma}_i$ ($i=x, y$) denote, respectively, a rotation around the z axis by $\varphi = n\pi/3$ and the mirror reflection with respect to the plane perpendicular to the i axis. Using Eq. (34) in Eq. (31), one can show that Eq. (32) holds for the four operations of Eq. (34). Similar considerations show that, besides $T_{\mathbf{R}}$, there are symmetry operations in Phase IV listed in the fourth row of Table II. Here the primitive cell is spanned by the basic vectors (19), thus containing a single circulation quantum. If $T_{\mathbf{R}}$ is identified with the usual translation operator, this space group can be labeled as $P6/mmm'$.⁴²

The same consideration is performed for every stable vortex phase found numerically. The results are summarized below in Table II.

B. Phase Transitions

The expansion (23) is also useful for enumerating possible transitions in vortex-lattice phases. Indeed, we can use the known results from the space group⁴³ using the correspondence $\exp(-\mathbf{R} \cdot \nabla) \leftrightarrow T_{\mathbf{R}}$ and (Bloch states) \leftrightarrow (magnetic Bloch states).

We first summarize basic features of the conventional Abrikosov lattices with a single order parameter within the framework of LLX:²⁶ (a) Any single $\mathbf{q} = \mathbf{q}_1$ suffices to describe them, due to broken translational symmetry of the vortex lattice. Each unit cell has a single circulation quantum κ . (b) The hexagonal (square) lattice is made up of $N = 6n$ ($4n$) Landau levels ($n = 0, 1, 2, \dots$), and the expansion coefficients $c_{N\mathbf{q}_1}$ can be chosen real. (c) More general structures are described by $N = 2n$ levels. Odd- N basis functions, some of which have finite amplitudes at the cores of even- N basis functions (see Appendix A), never participate in forming the order parameter, because such mixing is energetically unfavorable.

With multi-component order parameters, there can be a wide variety of vortices, which may be divided into two categories. I call the first category as “fill-core” states with a single circulation quantum per unit cell, i.e., only a single $\mathbf{q} = \mathbf{q}_1$ is relevant. Here the cores of the conventional Abrikosov lattice are filled in by some superfluid components using odd- N wavefunctions of Eq. (22). The second category may be called “shift-core” states, where core locations are not identical among different order-parameter components. The corresponding lattice has an enlarged unit cell with multiple circulation quanta. General structures with n_κ circulation quanta per unit cell can be described using n_κ different \mathbf{q} 's, and the unit cell becomes n_κ times as large as that of the conventional Abrikosov lattice. For example, structures with two quanta per unit cell can be described by choosing

$$\mathbf{q}_1 = \frac{\mathbf{b}_1 + \mathbf{b}_2}{2}, \quad \mathbf{q}_2 = \mathbf{0}, \quad (35)$$

where \mathbf{b}_1 and \mathbf{b}_2 are reciprocal lattice vectors defined by Eq. (20).

With these observations, we now realize that following second-order transitions are possible in a two-component system. (i) Deformation of a hexagonal or square lattice within a single- \mathbf{q} lattice. This accompanies entry of new even- N basis functions, and the coefficients $\{c_{N\mathbf{q}}\}$ become intrinsically complex. (ii) The entry of odd- N basis functions within a single- \mathbf{q} lattice, i.e. a transition into a fill-core lattice. Here, cores of even- N basis functions are filled in by some superfluid components not used in the bulk phase. The transition occurs below some critical angular velocity smaller than $\Omega_{c2}/3$. (iii) Mixing of another wave number \mathbf{q}_2 , i.e. a transition into a shift-core lattice. When applied to this system, the Lifshitz condition⁴³ concludes exclusively that $\mathbf{q}_2 - \mathbf{q}_1$ should be half a basic vector \mathbf{b}_j ($j = 1, 2$) of the reciprocal lattice, i.e. the only possibility is doubling of the unit cell.

Though not complete for the present nine-component system, the above list covers most of the transitions found below. The case (ii) corresponds to superfluid-core states such as the A-phase-core and double-core vortices in the B phase, whereas (iii) will be shown to describe a unit cell with two circulation quanta like the continuous unlocked vortex of the A phase.⁷ Since no odd-order couplings exist between $\tilde{A}_\mu^{(0)}$ and $(\tilde{A}_\nu^{(-1)}, \tilde{A}_\lambda^{(1)})$ in Eqs. (1)-(5), we also realize that a state of $\tilde{A}_\nu^{(-1)} \neq 0$ or $\tilde{A}_\lambda^{(1)} \neq 0$ accompanies a second-order transition as we decrease Ω from Ω_{c2} .

V. PHASE DIAGRAM FOR $0.01\Omega_{c2} \leq \Omega \leq \Omega_{c2}$

Figure 1 displays the obtained p - Ω phase diagram for $0.01\Omega_{c2} \leq \Omega \leq \Omega_{c2}$, where five different phases I-V are present. Symmetry properties of each phase, which have been clarified by group-theoretical considerations similar to that given around Eq. (34), are summarized in Table II. Also, critical values of the transitions are listed in Table III. Each phase is explained below in detail.

According to Eq. (17), the normal \rightarrow superfluid transition in rotation occurs at $\Omega_{c2} = \Omega_{c2}^{(0)}$ into $\tilde{A}_z^{(0)} \neq 0$. Thus, in Phase I just below Ω_{c2} , the polar state is realized to form the conventional hexagonal lattice as

$$\tilde{A}_z^{(0)} = \sqrt{V} \sum_N c_{N\mathbf{q}_1}^{(0)} \psi_{N\mathbf{q}_1} \quad (36)$$

with $N = 6n$ ($n = 0, 1, 2, \dots$), $\beta = \pi/3$, and $\rho = 1$. All $c_{N\mathbf{q}_1}^{(0)}$ can be put real, and \mathbf{q}_1 is conveniently chosen as Eq. (35) so that a core is located at the origin. As already discussed below Eq. (17), the stability of the polar state near Ω_{c2} can be attributed to its line node in the plane perpendicular to Ω which works favorably to reduce the kinetic energy dominant near Ω_{c2} . It follows from Eq. (28) that the \mathbf{d} -vector of Eq. (27) at $H = 0$ lies along an arbitrary direction in the xy plane which is fixed spontaneously. This degeneracy is lifted by a field in the plane so that $\mathbf{d} \perp \mathbf{H}$ is realized.

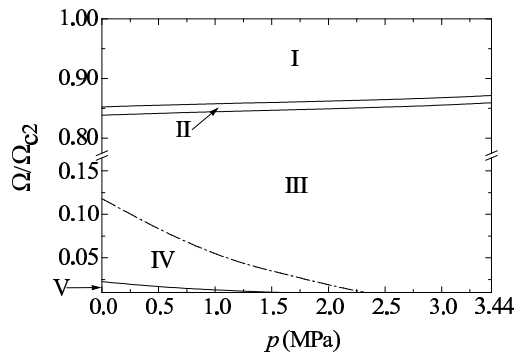


FIG. 1: The p - Ω phase diagram for $0.01 \leq \Omega/\Omega_{c2} \leq 1.0$. There are five different phases I-V. The III-IV transition is first-order corresponding to the A-B boundary in finite Ω , whereas the others are second-order.

TABLE II: Properties of Phases I-V. The notation of Ref. 42 is used for the point-group operations with $i = 1, 2, 3$, $m = x, y$, and $s = a, b$, and θ denotes the time-reversal operation. The point-group operations of Phases I and IV-VI are defined with respect to the origin. In contrast, those of Phases II and III are about the point $(\mathbf{a}_1 + \mathbf{a}_2)/2$ where a core of the SK sublattice is located, with x and y axes taken along $\mathbf{a}_1 + \mathbf{a}_2$ and $\mathbf{a}_1 - \mathbf{a}_2$, respectively. The operator $\{I|\mathbf{a}_1\}$, for example, denotes successive operations of the inversion and a magnetic translation by \mathbf{a}_1 , i.e., $\{I|\mathbf{a}_1\} \equiv T_{\mathbf{a}_1}I$.

Phase	unit cell	β	ρ	symmetry operations
I	$\mathbf{a}_1, \mathbf{a}_2$	$\pi/3$	1	$E, C_{6z}^{(\pm)}, C_{3z}^{(\pm)}, C_{2z}, I, S_{6z}^{(\pm)}, S_{3z}^{(\pm)}, \sigma_h, \theta C_{2i}', \theta C_{2i}'', \theta \sigma_{di}, \theta \sigma_{vi}$.
II	$\mathbf{a}_1 + \mathbf{a}_2, \mathbf{a}_1 - \mathbf{a}_2$	$\frac{\pi}{3} < \beta < \frac{\pi}{2}$	1	$E, C_{2z}, \{I \mathbf{a}_1\}, \{\sigma_h \mathbf{a}_1\}, \theta\{C_{2m} \mathbf{a}_1\}, \theta \sigma_m$.
III	$\mathbf{a}_1 + \mathbf{a}_2, \mathbf{a}_1 - \mathbf{a}_2$	$\pi/2$	1	$E, C_{4z}^{(\pm)}, C_{2z}, \{I \mathbf{a}_1\}, \{S_{4z}^{(\pm)} \mathbf{a}_1\}, \{\sigma_h \mathbf{a}_1\}, \theta\{C_{2m} \mathbf{a}_1\}, \theta\{C_{2s} \mathbf{a}_1\}, \theta \sigma_m, \theta \sigma_{ds}$.
IV	$\mathbf{a}_1, \mathbf{a}_2$	$\pi/3$	1	$E, C_{6z}^{(\pm)}, C_{3z}^{(\pm)}, C_2, I, S_{6z}^{(\pm)}, S_{3z}^{(\pm)}, \sigma_h, \theta C_{2i}', \theta C_{2i}'', \theta \sigma_{di}, \theta \sigma_{vi}$.
V	$\mathbf{a}_1, \mathbf{a}_2$	$\pi/3$	1	$E, C_{6z}^{(\pm)}, C_{3z}^{(\pm)}, C_{2z}, \theta \sigma_{di}, \theta \sigma_{vi}$.
VI	$\mathbf{a}_1, \mathbf{a}_2$	$\sim \pi/3$	~ 1	$E, C_{2z}, \theta \sigma_{dm}$.

TABLE III: Critical angular velocities of the phase transitions in units of Ω_{c2} .

p (MPa)	0	0.4	0.8	1.2	1.6	2.0	2.4	2.85	3.2	3.44
I-II	0.8527	0.8548	0.8569	0.8588	0.8605	0.8624	0.8644	0.8671	0.8696	0.8716
II-III	0.8388	0.8411	0.8433	0.8454	0.8473	0.8493	0.8515	0.8544	0.8572	0.8594
III-IV	1.18×10^{-1}	9.00×10^{-2}	6.54×10^{-2}	4.56×10^{-2}	3.16×10^{-2}	1.89×10^{-2}	8.32×10^{-3}	0.0	—	—
IV-V	2.23×10^{-2}	1.78×10^{-2}	1.44×10^{-2}	1.20×10^{-2}	1.05×10^{-2}	9.08×10^{-3}	7.78×10^{-3}	0.0	—	—

In Phase II, $\tilde{A}_z^{(\pm 1)}$ also become finite as⁴⁴

$$\tilde{A}_z^{(-1)} = \sqrt{V} \sum_N c_{N\mathbf{q}_2}^{(-1)} \psi_{N\mathbf{q}_2}, \quad (37a)$$

$$\tilde{A}_z^{(1)} = \sqrt{V} \sum_N c_{N\mathbf{q}_2}^{(1)} \psi_{N\mathbf{q}_2}. \quad (37b)$$

The N 's in Eqs. (36)-(37) are even numbers, and all the coefficients are essentially complex except $c_{0\mathbf{q}_1}^{(0)}$ which can be chosen real using a gauge transformation. The I-II transition is second-order corresponding to the SK line of Eq. (17). Indeed, $N=0$ and $N=2$ Landau levels are dominant in Eqs. (37a) and (37b), respectively. Due to the presence of $\tilde{A}_z^{(0)}$, however, the critical angular velocity $\Omega_c^{(I \leftrightarrow II)}$ is somewhat lowered from $\Omega_{c2}^{(-1)} = 0.9082\Omega_{c2}$ of Eq. (17), as seen in Fig. 1. The vector \mathbf{q}_2 is shifted from \mathbf{q}_1 by half a basic vector \mathbf{b}_j , so that the unit cell is doubled carrying two circulation quanta. Thus, Phase II is

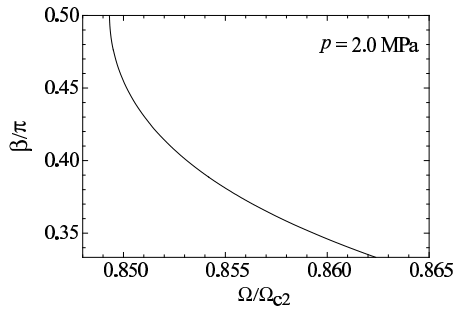


FIG. 2: The apex angle β as a function of Ω/Ω_{c2} at $p = 2.0$ MPa. Phase transitions occur at $\Omega_c^{(I \leftrightarrow II)} = 0.8623\Omega_{c2}$ and $\Omega_c^{(II \leftrightarrow III)} = 0.8493\Omega_{c2}$.

composed of interpenetrating polar and SK sublattices. This superposition with shifted core locations is energetically more favorable than that with the identical core locations, because $A_{\mu i}^* A_{\mu i}$ becomes finite everywhere. It is convenient to choose $\mathbf{q}_2 = \mathbf{0}$.⁴⁵ Then $\rho = 1$ holds throughout, and as seen in Fig. 2 calculated for $p = 2.0$ MPa, the apex angle β changes continuously throughout the phase between $\pi/3$ and $\pi/2$. This is a centered rectangular lattice with the primitive vectors given by $\mathbf{a}_1 \pm \mathbf{a}_2$. Figure 3 displays the order-parameter amplitudes at $p = 2.0$ MPa over $-a_2 \leq x, y \leq a_2$ for (a) $\Omega = 0.863\Omega_{c2}$ with $\beta = \pi/3$

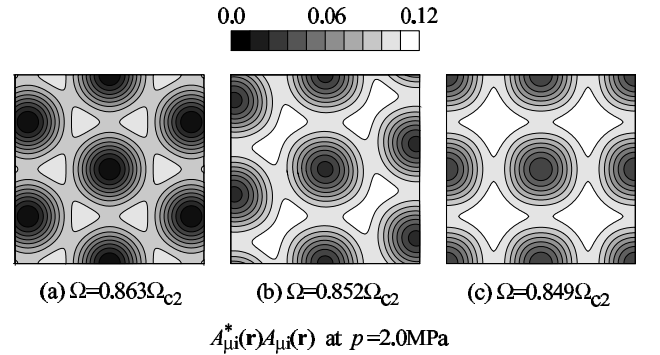


FIG. 3: The amplitude $\tilde{A}_{\mu i}^* \tilde{A}_{\mu i}$ normalized by the $\Omega = 0$ value over $-a_2 \leq x, y \leq a_2$ at $p = 2.0$ MPa. (a) At $\Omega = 0.863\Omega_{c2}$ where $\beta = \pi/3$ (polar state). (b) At $\Omega = 0.852\Omega_{c2}$ where $\beta = 0.414\pi$ (Phase II). (c) At $\Omega = 0.849\Omega_{c2}$ where $\beta = \pi/2$ (Phase III). Below $\Omega = 0.8623\Omega_{c2}$, the SK sublattice grows gradually with the largest amplitude at the cores of the polar sublattice. Thus, the amplitude $\tilde{A}_{\mu i}^* \tilde{A}_{\mu i}$ is finite everywhere in (b) and (c). The apex angle changes continuously from $\beta = \pi/3$ at $\Omega = 0.8623\Omega_{c2}$ to $\beta = \pi/2$ at $\Omega = 0.8493\Omega_{c2}$.

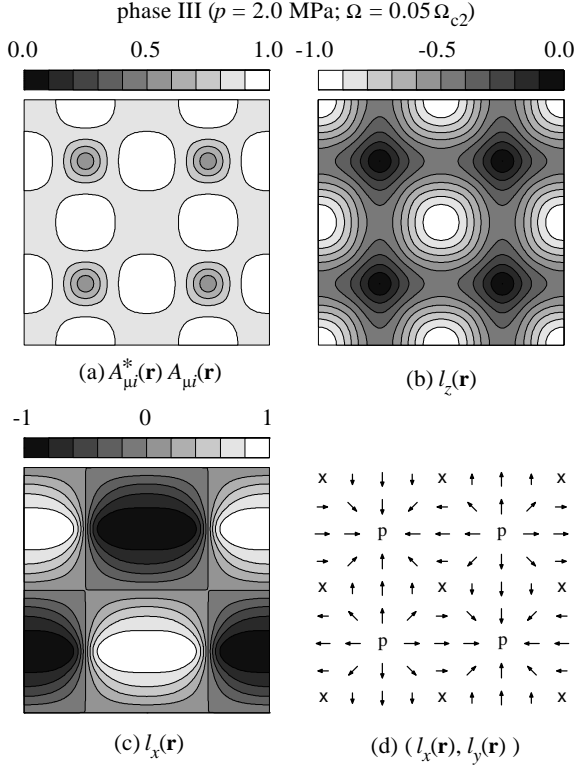


FIG. 4: Characteristic quantities in Phase III calculated over $-a_2 \leq x, y \leq a_2$ for $\Omega = 0.05 \Omega_{c2}$ at $p = 2.0$ MPa. (a) $\tilde{A}_{\mu i}^* \tilde{A}_{\mu i}$ normalized by the $\Omega = 0$ value. (b) $l_z(\mathbf{r})$. (c) $l_x(\mathbf{r})$. (d) Projection of $\mathbf{l}(\mathbf{r})$ onto the xy plane. The plot for $l_y(\mathbf{r})$ is obtained by rotating Fig. 4(c) by $-\pi/2$. The p and x sites in Fig. 4(d) correspond to the pure polar state and the pure ABM state with $l_z = -1$, respectively.

(still in polar state), (b) $\Omega = 0.852 \Omega_{c2}$ with $\beta = 0.414\pi$ (Phase II), and (c) $\Omega = 0.849 \Omega_{c2}$ with $\beta = \pi/2$ (just below the II-III boundary). We observe that the SK state grows gradually from $\Omega = 0.8623 \Omega_{c2}$ with the largest amplitude at the cores of the polar state. The \mathbf{d} -vector has the same character as Phase I.

In Phase III, the system remains in the square lattice with $\beta = \pi/2$ and $\rho = 1$. Only $N = 4n, 4n, \text{ and } 4n+2$ ($n = 0, 1, 2, \dots$) Landau levels are relevant in Eqs. (36), (37a), and (37b), respectively. Whereas all $c_{N\mathbf{q}_1}^{(0)}$'s can be put real, the coefficients $c_{N\mathbf{q}_2}^{(\mp 1)}$ are complex with a common phase $-\pi/4$ relative to $c_{0\mathbf{q}_1}^{(0)}$. The II-III transition is second-order, as may be realized from the square-root behavior of Fig. 2. As Ω is decreased from the boundary, the SK sublattice with the coefficients $c_{N\mathbf{q}_2}^{(\mp 1)}$ grows rapidly. Also within the SK sublattice, the ABM⁽⁺⁾ component with the coefficients $c_{N\mathbf{q}_2}^{(1)}$ becomes less important at lower Ω so that the sublattice approaches to the pure ABM state with $l_z = -1$. Figures 4(a)-(d) display the order-parameter amplitude (30a) and the orbital angular momentum (30c) calculated over $-a_2 \leq x, y \leq a_2$ for

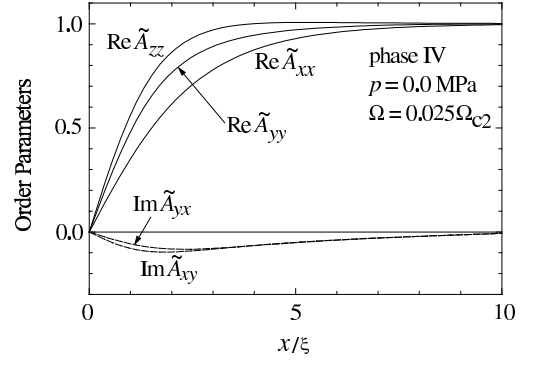


FIG. 5: Order parameters of Phase IV along x axis at $p = 0.0$ MPa and $\Omega = 0.025 \Omega_{c2}$. The amplitudes are normalized by the $\Omega = 0$ value of \tilde{A}_{xx} , and the common phase $\pi/8$ is subtracted from $\tilde{A}_{\mu i}$.

$\Omega = 0.05 \Omega_{c2}$ at $p = 2.0$ MPa. We realize from these figures that Phase III at lower Ω is essentially the A-phase mixed-twist lattice with polar cores and double circulation quanta per unit cell.^{1,46} Indeed, as seen in Fig. 4(d), the \mathbf{l} -vector rotates from downward at the origin to horizontally outward or inward towards polar cores. A group-theoretical consideration, similar to that given around Eq. (34), clarifies that this phase is characterized by the symmetry operations given in the third row of Table II; they are defined with respect to a polar core, i.e., p site of Fig. 4(d). It is worth comparing Fig. 4 with Fig. 3(c) at $\Omega = 0.849 \Omega_{c2}$. The cores at $\Omega = 0.849 \Omega_{c2}$ now acquire a large ABM amplitude with $l_z = -1$, and the points with the maximum polar amplitude at $\Omega = 0.849 \Omega_{c2}$ turn into cores, i.e., singular points of the vector field $\mathbf{l}(\mathbf{r})$ where the amplitude $\tilde{A}_{\mu i}^* \tilde{A}_{\mu i}$ is also smallest. Notice that this phase is stable at all pressures. It is also worth pointing out that, although both carrying double quanta per unit cell, this structure is completely different from the vortex-sheet-like structure found in a two-component system.²⁸ The \mathbf{d} -vector has the same character as Phase I.

Phase IV is a hexagonal lattice of the B-phase normal-core vortex or o-vortex, which was found in the isolated-vortex calculation by Ohmi, Tsuneto, and Fujita.¹⁹ However, it was concluded later by another isolated-vortex calculation¹⁰ that this normal-core vortex is a metastable state. Indeed, the vortex has never been observed experimentally. The present calculation shows, however, that it will be stabilized as we increase Ω . The non-zero components besides Eq. (36) are given by

$$\tilde{A}_x^{(-1)} = \sqrt{V} \sum_N [c_{N\mathbf{q}_1}^{(-1)} \psi_{N\mathbf{q}_1} + c_{N+4\mathbf{q}_1}^{(-1)} \psi_{N+4\mathbf{q}_1}], \quad (38a)$$

$$\tilde{A}_y^{(-1)} = i\sqrt{V} \sum_N [c_{N\mathbf{q}_1}^{(-1)} \psi_{N\mathbf{q}_1} - c_{N+4\mathbf{q}_1}^{(-1)} \psi_{N+4\mathbf{q}_1}], \quad (38b)$$

$$\tilde{A}_x^{(1)} = \sqrt{V} \sum_N [c_{N\mathbf{q}_1}^{(1)} \psi_{N\mathbf{q}_1} + c_{N+2\mathbf{q}_1}^{(1)} \psi_{N+2\mathbf{q}_1}], \quad (38c)$$

$$\tilde{A}_y^{(1)} = -i\sqrt{V} \sum_N [c_{N\mathbf{q}_1}^{(1)} \psi_{N\mathbf{q}_1} - c_{N+2\mathbf{q}_1}^{(1)} \psi_{N+2\mathbf{q}_1}], \quad (38d)$$

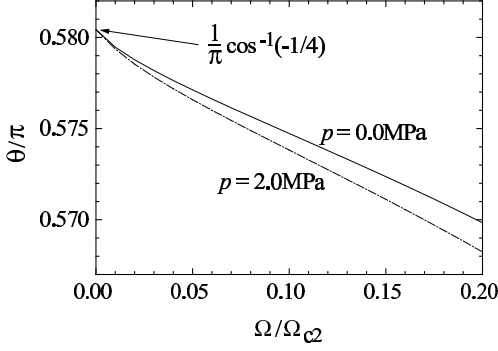


FIG. 6: Rotation angle θ defined by Eq. (39) as a function of Ω/Ω_{c2} . It is calculated beyond the III-IV boundary in Fig. 1 into the metastable region.

where $N = 6n$, $\beta = \pi/3$, $\rho = 1$, and all the coefficients are real. Figure 5 plots the order-parameter amplitudes along x direction calculated for $\Omega = 0.025\Omega_{c2}$ at $p = 0.0$ MPa. They already display the same features as those obtained by the isolated-vortex calculations.^{10,11,19} The III-IV boundary in Fig. 1 is a first-order-transition line, approaching towards $p = p_{pcp}$ at $\Omega = 0$ and vanishing for $p > p_{pcp}$, as expected. Thus, this line may be regarded as the A-B phase boundary in finite Ω . It is convenient here to parameterize the rotation matrix \underline{R} of Eq. (12) as¹

$$R_{\mu\nu} = \delta_{\mu\nu} \cos \theta + n_\mu n_\nu (1 - \cos \theta) - \varepsilon_{\mu\nu\lambda} n_\lambda \sin \theta, \quad (39)$$

where \mathbf{n} is a unit vector. Then it is found that, as Ω is decreased, the rotation angle θ approaches from below to the bulk value $\cos^{-1}(-1/4)$, as seen in Fig. 6. The \mathbf{n} -vector at $H = 0$ lies along an arbitrary direction in the xy plane which is fixed spontaneously. Upon applying the magnetic field in the plane, the state $\mathbf{n} \parallel \mathbf{H}$ is realized.

Phase V continuously fills in Phase-IV core regions with the superfluid components not used in Phase IV. Besides those of Phase IV, the solution indeed has new non-zero components which are made up only of odd Landau levels as

$$\tilde{A}_x^{(0)} = \sqrt{V} \sum_N [c_{N+1\mathbf{q}_1}^{(0)} \psi_{N+1\mathbf{q}_1} + c_{N+5\mathbf{q}_1}^{(0)} \psi_{N+5\mathbf{q}_1}], \quad (40a)$$

$$\tilde{A}_y^{(0)} = i\sqrt{V} \sum_N [c_{N+1\mathbf{q}_1}^{(0)} \psi_{N+1\mathbf{q}_1} - c_{N+5\mathbf{q}_1}^{(0)} \psi_{N+5\mathbf{q}_1}], \quad (40b)$$

$$\tilde{A}_z^{(-1)} = \sqrt{V} \sum_N c_{N+5\mathbf{q}_1}^{(-1)} \psi_{N+5\mathbf{q}_1}, \quad (40c)$$

$$\tilde{A}_z^{(1)} = \sqrt{V} \sum_N c_{N+1\mathbf{q}_1}^{(1)} \psi_{N+1\mathbf{q}_1}, \quad (40d)$$

where $N = 6n$, $\beta = \pi/3$, $\rho = 1$, and all the coefficients are real. Figure 7 plots the order-parameter amplitudes along x direction calculated for $\Omega = 0.01\Omega_{c2}$ at $p = 0.0$ MPa. The core superfluid components satisfy $\text{Re}\tilde{A}_{zx} = \text{Im}\tilde{A}_{zy}$ and $\text{Re}\tilde{A}_{xz} = \text{Im}\tilde{A}_{yz}$ at the origin. As

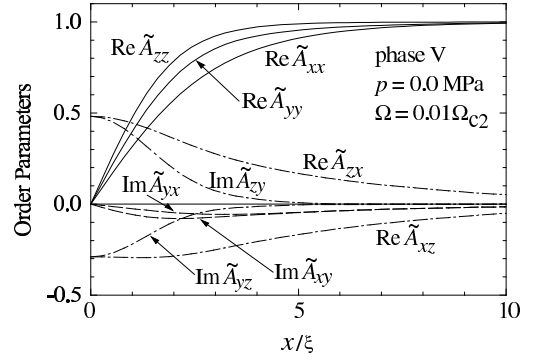


FIG. 7: Order parameters of Phase V along x axis at $p = 0.0$ MPa and $\Omega = 0.01\Omega_{c2}$. The amplitudes are normalized by the $\Omega = 0$ value of \tilde{A}_{xx} , and the common phase $\pi/8$ is subtracted from $\tilde{A}_{\mu i}$. The equalities $\text{Re}\tilde{A}_{zx} = \text{Im}\tilde{A}_{zy}$ and $\text{Re}\tilde{A}_{xz} = \text{Im}\tilde{A}_{yz}$ hold at $x = 0$.

may be realized from this figure, this state corresponds to the A-phase-core vortex or axisymmetric v-vortex found theoretically by Salomaa and Volovik,¹⁰ which also has been observed experimentally.^{8,9} Indeed, using the properties of $\psi_{N\mathbf{q}_1}$ given in Eq. (A8), one can show that the order-parameter matrix $\tilde{A} \equiv (\tilde{A}_{\mu i})$ satisfies Eqs. (34a)-(34c) but not Eq. (34d). Thus, the present calculation has clarified for the first time that a vortex lattice with superfluid cores can be described by a superposition of odd Landau levels. The IV-V phase boundary is a second-order transition, as anticipated by Salomaa and Volovik based on a single-vortex consideration,¹⁰ which is driven mainly by the $N = 1$ Landau level. Due to the presence of finite order parameters composed of even Landau levels, however, the critical angular velocity $\Omega_c^{(IV \leftrightarrow V)}$ is lowered from $\Omega_{c2}/3$ expected for the pure $N = 1$ Landau level to become smaller than $\sim 2 \times 10^{-2}\Omega_{c2}$ rad/s, as seen in Fig. 1. The \mathbf{n} -vector has the same character as Phase IV.

VI. TRANSITION BETWEEN A-PHASE-CORE AND DOUBLE-CORE LATTICES

Using the same parameters as those given in Table I, Thuneberg¹¹ carried out an isolated-vortex calculation. He thereby succeeded in identifying two kinds of vortices experimentally found in the B phase near Ω_{c1} . According to his calculation, the double-core vortex is stable below about 2.5 MPa over the A-phase-core vortex. Combining his result with the phase diagram of Fig. 1, we naturally anticipate another phase transition below $0.01\Omega_{c2}$ from the A-phase-core lattice to the double-core lattice at low pressures.

To find the transition, I have performed a variational calculation down to $\Omega = 0.0001\Omega_{c2}$ at $p = 0.0$ MPa using $N \leq 3000$ Landau levels. The hexagonal lattice is assumed to simplify the calculation, and I have taken

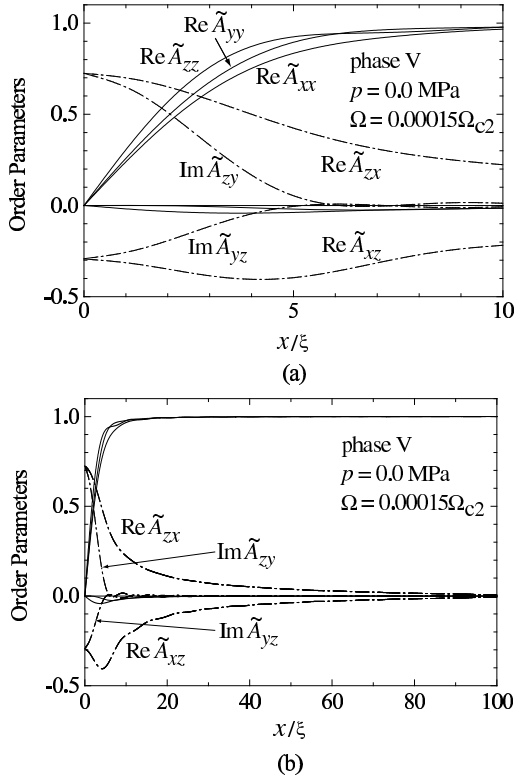


FIG. 8: Order parameters along x axis at $p = 0.0$ MPa and $\Omega = 0.00015\Omega_{c2}$. (a) $0 \leq x/\xi \leq 10$. (b) $0 \leq x/\xi \leq 100$. The amplitudes are normalized by the $\Omega = 0$ value of \tilde{A}_{xx} , and the common phase $\pi/8$ is subtracted from $\tilde{A}_{\mu i}$. The relations $\text{Re}\tilde{A}_{zx} = \text{Im}\tilde{A}_{zy}$ and $\text{Re}\tilde{A}_{xz} = \text{Im}\tilde{A}_{yz}$ still hold at $x = 0$.

72×72 integration points of equal interval per unit cell. It has been checked that increasing integration points further does not change F beyond 10^{-8} order. Unfortunately, however, $N \leq 3000$ Landau levels at $0.0001\Omega_{c2}$ are still not enough to obtain enough convergence. Indeed, it has been observed that including more Landau levels as $N \leq 1800, 2400, 3000$ change the amplitudes of the core superfluid components to a noticeable level and lower the critical angular velocity of the transition. Also, since the isolated double-core vortex has only a discrete π -rotational symmetry about z axis, the double-core lattice is expected to deform spontaneously from the hexagonal structure. Thus, the present calculation is a variational one to clarify the nature of the transition as well as to estimate an upper bound for the critical Ω . It should be noted, however, that assuming the hexagonal lattice hardly change the free energy in this low- Ω region with a large intervortex distance, and does not affect the critical Ω if the transition happens to be second-order.

Figure 8 displays the order parameters along x axis at $p = 0.0$ MPa and $\Omega = 0.00015\Omega_{c2}$. The relations $\text{Re}\tilde{A}_{zx}(\mathbf{0}) = \text{Im}\tilde{A}_{zy}(\mathbf{0})$ and $\text{Re}\tilde{A}_{xz}(\mathbf{0}) = \text{Im}\tilde{A}_{yz}(\mathbf{0})$ still hold; hence the system remains in Phase V of the A-phase-core lattice. Comparing Fig. 8(a) with Fig. 7, we observe that the core superfluid components have grown

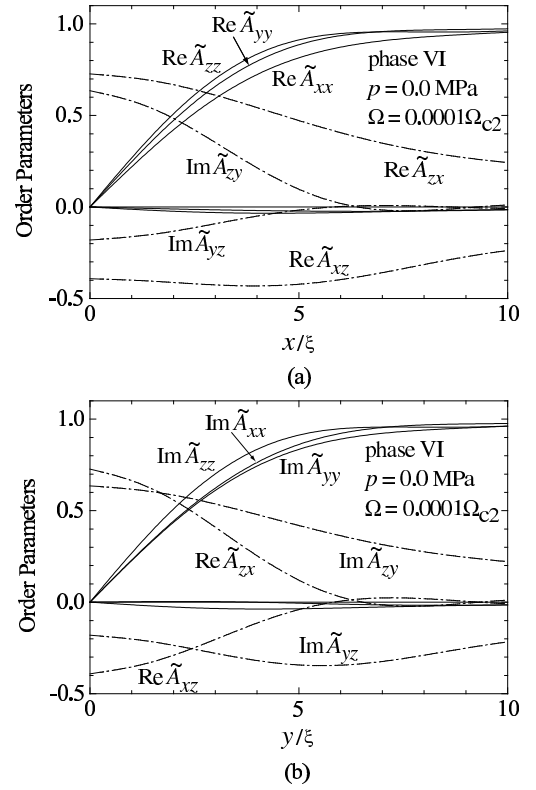


FIG. 9: Order parameters at $p = 0.0$ MPa and $\Omega = 0.0001\Omega_{c2}$. (a) Along x axis over $0 \leq x/\xi \leq 10$; (b) along y axis over $0 \leq y/\xi \leq 10$. The amplitudes are normalized by the $\Omega = 0$ value of \tilde{A}_{xx} , and the common phase $\pi/8$ is subtracted from $\tilde{A}_{\mu i}$. Notice $\text{Re}\tilde{A}_{zx}(\mathbf{0}) \neq \text{Im}\tilde{A}_{zy}(\mathbf{0})$ and $\text{Re}\tilde{A}_{xz}(\mathbf{0}) \neq \text{Im}\tilde{A}_{yz}(\mathbf{0})$, indicating the double-core vortex.

substantially, and the bulk components \tilde{A}_{xx} , \tilde{A}_{yy} , and \tilde{A}_{zz} are somewhat depleted in the core region. However, Fig. 8(b) shown over the longer distance $0 \leq x/\xi \leq 100$ indicates that the requirement $\text{Re}\tilde{A}_{xz}(\mathbf{0}) = \text{Im}\tilde{A}_{yz}(\mathbf{0})$ of the A-phase-core vortex is unfavorable for a further growth of $\text{Re}\tilde{A}_{zx}$. Thus, we see clearly that the system wants to break the symmetry of the A-phase-core vortex around $\Omega \sim 0.00015\Omega_{c2}$.

Figure 9 shows the order parameters for a slightly lower $\Omega = 0.0001\Omega_{c2}$ at $p = 0.0$ MPa along (a) x axis and (b) y axis. Here the symmetry of the A-phase-core vortex is manifestly broken as $\text{Re}\tilde{A}_{xz}(\mathbf{0}) \neq \text{Im}\tilde{A}_{yz}(\mathbf{0})$ and $\text{Re}\tilde{A}_{zx}(\mathbf{0}) \neq \text{Im}\tilde{A}_{zy}(\mathbf{0})$. Thus, the double-core lattice, also called Phase VI, is realized. Indeed, these $\tilde{A}_{\mu i}$ have the same qualitative features as those of the isolated double-core vortex calculated by Thuneberg.¹¹ The order parameters are given explicitly by

$$\tilde{A}_z^{(0)} = \sqrt{V} \sum_N c_{N\mathbf{q}_1}^{(0)} \psi_{N\mathbf{q}_1}, \quad (41a)$$

$$\begin{aligned}\tilde{A}_x^{(-1)} &= \sqrt{V} \sum_N [c_{N\mathbf{q}_1}^{(-1)} \psi_{N\mathbf{q}_1} + c_{N+4\mathbf{q}_1}^{(-1)} \psi_{N+4\mathbf{q}_1}] \\ &\quad + \sqrt{V} \sum_N [d_{N\mathbf{q}_1}^{(-1)} \psi_{N\mathbf{q}_1} + d_{N+4\mathbf{q}_1}^{(-1)} \psi_{N+4\mathbf{q}_1}],\end{aligned}\quad (41b)$$

$$\begin{aligned}\tilde{A}_y^{(-1)} &= i\sqrt{V} \sum_N [c_{N\mathbf{q}_1}^{(-1)} \psi_{N\mathbf{q}_1} - c_{N+4\mathbf{q}_1}^{(-1)} \psi_{N+4\mathbf{q}_1}] \\ &\quad - i\sqrt{V} \sum_N [d_{N\mathbf{q}_1}^{(-1)} \psi_{N\mathbf{q}_1} - d_{N+4\mathbf{q}_1}^{(-1)} \psi_{N+4\mathbf{q}_1}],\end{aligned}\quad (41c)$$

$$\begin{aligned}\tilde{A}_x^{(1)} &= \sqrt{V} \sum_N [c_{N\mathbf{q}_1}^{(1)} \psi_{N\mathbf{q}_1} + c_{N+2\mathbf{q}_1}^{(1)} \psi_{N+2\mathbf{q}_1}] \\ &\quad + \sqrt{V} \sum_N [d_{N\mathbf{q}_1}^{(1)} \psi_{N\mathbf{q}_1} + d_{N+2\mathbf{q}_1}^{(1)} \psi_{N+2\mathbf{q}_1}],\end{aligned}\quad (41d)$$

$$\begin{aligned}\tilde{A}_y^{(1)} &= -i\sqrt{V} \sum_N [c_{N\mathbf{q}_1}^{(1)} \psi_{N\mathbf{q}_1} - c_{N+2\mathbf{q}_1}^{(1)} \psi_{N+2\mathbf{q}_1}] \\ &\quad + i\sqrt{V} \sum_N [d_{N\mathbf{q}_1}^{(1)} \psi_{N\mathbf{q}_1} - d_{N+2\mathbf{q}_1}^{(1)} \psi_{N+2\mathbf{q}_1}],\end{aligned}\quad (41e)$$

$$\begin{aligned}\tilde{A}_x^{(0)} &= \sqrt{V} \sum_N [c_{N+1\mathbf{q}_1}^{(0)} \psi_{N+1\mathbf{q}_1} + c_{N+5\mathbf{q}_1}^{(0)} \psi_{N+5\mathbf{q}_1}] \\ &\quad + \sqrt{V} \sum_N [d_{N+1\mathbf{q}_1}^{(0)} \psi_{N+1\mathbf{q}_1} + d_{N+5\mathbf{q}_1}^{(0)} \psi_{N+5\mathbf{q}_1}],\end{aligned}\quad (41f)$$

$$\begin{aligned}\tilde{A}_y^{(0)} &= i\sqrt{V} \sum_N [c_{N+1\mathbf{q}_1}^{(0)} \psi_{N+1\mathbf{q}_1} - c_{N+5\mathbf{q}_1}^{(0)} \psi_{N+5\mathbf{q}_1}] \\ &\quad - i\sqrt{V} \sum_N [d_{N+1\mathbf{q}_1}^{(0)} \psi_{N+1\mathbf{q}_1} - d_{N+5\mathbf{q}_1}^{(0)} \psi_{N+5\mathbf{q}_1}],\end{aligned}\quad (41g)$$

$$\tilde{A}_z^{(-1)} = \sqrt{V} \sum_N [c_{N+5\mathbf{q}_1}^{(-1)} \psi_{N+5\mathbf{q}_1} + d_{N+1\mathbf{q}_1}^{(-1)} \psi_{N+1\mathbf{q}_1}],\quad (41h)$$

$$\tilde{A}_z^{(1)} = \sqrt{V} \sum_N [c_{N+1\mathbf{q}_1}^{(1)} \psi_{N+1\mathbf{q}_1} + d_{N+5\mathbf{q}_1}^{(1)} \psi_{N+5\mathbf{q}_1}],\quad (41i)$$

with $N = 6n$, $\beta = \pi/3$, and $\rho = 1$. All the coefficients are real, and terms with $d_{N\mathbf{q}_1}^{(m)}$, which are absent in the A-phase-core vortex, bring new asymmetry between $\tilde{A}_x^{(m)}$ and $\tilde{A}_y^{(m)}$ as well as new terms in $\tilde{A}_z^{(\mp 1)}$.

It follows from Figs. 8 and 9 that a phase transition occurs between $\Omega = 0.00015\Omega_{c2}$ and $\Omega = 0.0001\Omega_{c2}$ at $p = 0.0$ MPa. As already noted, however, $N \leq 3000$ Landau levels are still not enough to identify the critical value $\Omega_c^{(V \leftrightarrow VI)}$ or the order of the transition. Including more Landau levels has been observed to decrease $\Omega_c^{(V \leftrightarrow VI)}$, so that the present value $\Omega_c^{(V \leftrightarrow VI)} \approx 0.0001\Omega_{c2}$ should be considered as an upper bound for $\Omega_c^{(V \leftrightarrow VI)}$ at $p = 0.0$ MPa. It is also expected from Fig. 1 that $\Omega_c^{(V \leftrightarrow VI)}(p)$ is a decreasing function of p . As for the order of the transition, the isolated-vortex calculation by Thuneberg¹¹ clarified that it is first-order near Ω_{c1} . However, it can be second-order from a purely group-theoretical viewpoint. Therefore, it is possible that the transition at $p = 0.0$ MPa is second-order, changing its nature into first-order through a tricritical point⁴³ as we increase p .

Experimentally, the present result implies that, as we increase Ω above 3 rad/s, the double-core region will shrink in the p - T plane to be replaced by the A-

phase-core region, vanishing eventually in a rotation of $10^3 \sim 10^4$ rad/s. In addition, the phase boundary between the double-core and A-phase-core vortices may change its character from first-order to second-order in increasing Ω . A systematic study for $\Omega \lesssim 10^2$ rad/s may be able to detect this shrinkage of the double-core region as well as to provide an estimate for the critical Ω where the double-core vortex disappears.

VII. SUMMARY

Based on a new approach starting from Ω_{c2} down towards Ω_{c1} , the present calculation has revealed a rich phase diagram of rapidly rotating superfluid ^3He . Six phases have been found in the p - Ω plane, and we now have a complete story of how the polar hexagonal lattice near Ω_{c2} develops into the A-phase-core and double-core vortices experimentally observed in the B phase. Interestingly, the polar or the ABM state is favorable over the isotropic Balian-Werthamer state for $\Omega \gtrsim 0.1\Omega_{c2}$.

The present study have also clarified prototypes of vortices expected in multicomponent superfluids and superconductors. With multiple order parameters, it is possible, and may be energetically favorable, to fill cores of an existing component with others not used yet. These unconventional vortices have been classified here into two categories, i.e., “shift-core” and “fill-core” states. The former vortex lattices are composed of interpenetrating sublattices of different components which can be described by using multiple magnetic Bloch vectors $(\mathbf{q}_1, \mathbf{q}_2, \dots)$. They have an enlarged unit cell with multiple circulation quanta. This category includes Phase III of Fig. 1 where the mixed-twist lattice is realized at low Ω , and also, the vortex sheet expected in two-component systems.^{28,30} In both cases, spatial variation of the l-vector is the main origin of vorticity. The latter vortex lattices, which may be realized for $\Omega \lesssim \Omega_{c2}/3$, can be described using odd N Landau levels with the same magnetic Bloch vector. This includes the A-phase-core and double-core lattices in the B phase.

Superfluid ^3He is a unique system with 9 order parameters without intrinsic anisotropies. In spite of every difficulty to realize $\Omega_{c2} \sim (1 - T/T_c) \times 10^7$, the whole phase diagram over $0 \leq \Omega \leq \Omega_{c2}$ is worth establishing experimentally to advance our knowledge on unconventional vortices. As a first step of this project, however, it may not be so difficult to observe shrinkage of the double-core region in the p - T plane in increasing Ω . Observations of vanishing double-core region in the p - T plane and the appearance of the normal-core vortex will mark next two stages. To realize Ω_{c2} , it will be necessary either to acquire $\Omega \sim 10^3$ - 10^7 rad/s at low temperatures or to perform accurate experiments in the region $1 - T/T_c \sim 10^{-3}$ - 10^{-8} . In the former case, the sample size should be made adequately small to keep the pressure constant over it; for example, $\Delta p = 0.1$ MPa at $\Omega = 10^6$ rad/s for the sample radius of $R = 5 \times 10^{-5}$ m.

Theoretically, it still remains as a future problem to establish a complete phase diagram of the A-phase region, i.e., how the mixed-twist lattice of Phase III grows into either of the locked vortex 1, the continuous unlocked vortex, the singular vortex, or the vortex sheet, which have been established by low- Ω calculations.⁷ This fact also implies that there may be multiple unknown phases waiting to be discovered experimentally in moderate Ω .

Acknowledgments

It is a great pleasure to acknowledge enlightening discussions with and/or comments from V. Eltsov, M. Fogelström, M. Krusius, N. Schopohl, E. Thuneberg, G. E. Volovik, and P. Wölfle. This research is supported by Grant-in-Aid for Scientific Research from the Ministry of Education, Culture, Sports, Science, and Technology of Japan.

APPENDIX A: PROPERTIES OF $\psi_{N\mathbf{q}}$

(i) The basis functions satisfy the orthonormality:

$$\begin{cases} \langle \psi_{N\mathbf{q}} | \psi_{N'\mathbf{q}'} \rangle = \delta_{NN'} \delta_{\mathbf{q}\mathbf{q}'} \\ \sum_{N\mathbf{q}} |\psi_{N\mathbf{q}} \rangle \langle \psi_{N\mathbf{q}}| = 1 \end{cases} \quad (\text{A1})$$

(ii) Upon applying Eq. (18) with $\mathbf{R} \equiv n_1 \mathbf{a}_1 + n_2 \mathbf{a}_2$, the basis function $\psi_{N\mathbf{q}}$ is transformed as

$$T_{\mathbf{R}} \psi_{N\mathbf{q}}(\mathbf{r}) = e^{-i\mathbf{q}\cdot\mathbf{R} - i\pi n_1 n_2} \psi_{N\mathbf{q}}(\mathbf{r}). \quad (\text{A2})$$

(iii) The function $\psi_{N\mathbf{q}}$ is obtained from $\psi_{N\mathbf{0}}$ by a magnetic translation as

$$\psi_{N\mathbf{q}}(\mathbf{r}) = T_{l_c^2 \mathbf{q} \times \hat{\mathbf{z}}} \psi_{N\mathbf{0}}(\mathbf{r}). \quad (\text{A3})$$

It thus follows that $\psi_{N\mathbf{q}}$ and $\psi_{N\mathbf{q}'}$ are essentially the same function, differing only in the location of zeros.

(iv) The basis function $\psi_{N\mathbf{q}}(\mathbf{r})$ vanishes at

$$\mathbf{r} = \frac{\mathbf{R}}{2} - l_c^2 \mathbf{q} \times \hat{\mathbf{z}} \quad \text{for} \quad \begin{cases} n_1 n_2 = \text{odd}; & N: \text{even}, \\ n_1 n_2 = \text{even}; & N: \text{odd}. \end{cases} \quad (\text{A4})$$

Thus, $\psi_{N\mathbf{q}_1}(\mathbf{0}) = 0$ for $\mathbf{q}_1 \equiv (\mathbf{b}_1 + \mathbf{b}_2)/2$ and $N = 2n$.

(v) Generally, $\psi_{N\mathbf{q}_1}(\mathbf{r})$ and $\psi_{N\mathbf{0}}(\mathbf{r})$ at least satisfy

$$\begin{cases} \psi_{N\mathbf{q}_1}(-\mathbf{r}) = e^{i(N-1)\pi} \psi_{N\mathbf{q}_1}(\mathbf{r}) \\ \psi_{N\mathbf{0}}(-\mathbf{r}) = e^{iN\pi} \psi_{N\mathbf{0}}(\mathbf{r}) \end{cases} \quad (\text{A5})$$

(vi) For centered rectangular lattices with $\rho = 1$, $\psi_{N\mathbf{q}}(\mathbf{r})$'s for $\mathbf{q} = \mathbf{0}$ and \mathbf{q}_1 satisfy, in addition to Eq. (A5), the following equality corresponding to the mirror reflection with respect to the plane including \mathbf{z} and $\mathbf{a}_1 + \mathbf{a}_2$:

$$\begin{aligned} & \psi_{N\mathbf{q}}(-x \cos \beta + y \sin \beta, x \sin \beta + y \cos \beta) \\ &= \exp(-i\varphi_{N\mathbf{q}}) \psi_{N\mathbf{q}}^*(x, y), \end{aligned} \quad (\text{A6})$$

where $\varphi_{N\mathbf{q}}$ is a constant which does not depend on \mathbf{r} .

(vii) For the square lattice with $\beta = \pi/2$ and $\rho = 1$, the basis functions $\psi_{N\mathbf{q}_1}(\mathbf{r})$ and $\psi_{N\mathbf{0}}(\mathbf{r})$ satisfy

$$\begin{cases} \psi_{N\mathbf{q}_1}(\underline{R}_\varphi^{-1} \mathbf{r}) = e^{i(N-1)\varphi} \psi_{N\mathbf{q}_1}(\mathbf{r}) \\ \psi_{N\mathbf{q}_1}(x, -y) = e^{i\pi/2} \psi_{N\mathbf{q}_1}^*(x, y) \\ \psi_{N\mathbf{q}_1}(y, x) = e^{-i\pi(N-2)/2} \psi_{N\mathbf{q}_1}^*(x, y) \\ \psi_{N\mathbf{0}}(\underline{R}_\varphi^{-1} \mathbf{r}) = e^{iN\varphi} \psi_{N\mathbf{0}}(\mathbf{r}) \\ \psi_{N\mathbf{0}}(x, -y) = \psi_{N\mathbf{0}}^*(x, y) \\ \psi_{N\mathbf{0}}(y, x) = e^{-i\pi N/2} \psi_{N\mathbf{0}}^*(x, y) \end{cases} \quad (\text{A7})$$

where \underline{R}_φ denotes a rotation around z axis by $\varphi = n\pi/2$. It hence follows that $\psi_{N\mathbf{q}_1}(\mathbf{0}) = 0$ except $N = 4n + 1$, and $\psi_{N\mathbf{0}}(\mathbf{0}) = 0$ except $N = 4n$.

(viii) For the hexagonal lattice with $\beta = \pi/3$ and $\rho = 1$, the basis function $\psi_{N\mathbf{q}_1}(\mathbf{r})$ satisfies

$$\begin{cases} \psi_{N\mathbf{q}_1}(\underline{R}_\varphi^{-1} \mathbf{r}) = e^{i(N-1)\varphi} \psi_{N\mathbf{q}_1}(\mathbf{r}) \\ \psi_{N\mathbf{q}_1}(x, -y) = e^{i\pi/4} \psi_{N\mathbf{q}_1}^*(x, y) \\ \psi_{N\mathbf{q}_1}(-x, y) = e^{i\pi/4 + i(N-1)\pi} \psi_{N\mathbf{q}_1}^*(x, y) \end{cases} \quad (\text{A8})$$

where $\varphi = n\pi/3$. Thus, $\psi_{N\mathbf{q}_1}(\mathbf{0}) = 0$ except $N = 6n + 1$.

* URL: <http://phys.sci.hokudai.ac.jp/~kita/index-e.html>; Electronic address: kita@phys.sci.hokudai.ac.jp

¹ A. L. Fetter, in *Progress in Low Temperature Physics Vol. X*, ed. by D. F. Brewer (North-Holland, Amsterdam, 1986) p. 1.

² M. M. Salomaa and G. E. Volovik, *Rev. Mod. Phys.* **59**, 533 (1987); **60**, 573 (1988).

³ P. Hakonen, O. V. Lounasmaa, and J. Simola, *Physica B* **160**, 1 (1989).

⁴ D. Vollhardt and P. Wölfle, *The Superfluid Phases of He-*

lium 3 (Taylor & Francis, London, 1990).

⁵ G. E. Volovik, *Exotic Properties of Superfluid ³He* (World Scientific, Singapore, 1992).

⁶ M. Krusius, *J. Low Temp. Phys.* **91**, 233 (1993).

⁷ O. V. Lounasmaa and E. V. Thuneberg, *Proc. Natl. Acad. Sci. USA* **96**, 7760 (1999); available at <http://www.pnas.org>.

⁸ O. T. Ikkala, G. E. Volovik, P. J. Hakonen, Y. M. Bunkov, S. T. Islander, and G. A. Kharadze, *JETP Lett.* **35**, 416 (1982).

- ⁹ P. J. Hakonen, M. Krusius, M. M. Salomaa, J. T. Simola, Y. M. Bunkov, V. P. Mineev, and G. E. Volovik, Phys. Rev. Lett. **51**, 1362 (1983).
- ¹⁰ M. M. Salomaa and G.E. Volovik, Phys. Rev. Lett. **51**, 2040 (1983); Phys. Rev. **B31**, 203 (1985).
- ¹¹ E. V. Thuneberg, Phys. Rev. **B36**, 3583 (1987).
- ¹² T. Fujita, M. Nakahara, T. Ohmi, and T. Tsuneto, Prog. Theoret. Phys. **60**, 671 (1978).
- ¹³ J. P. Pekola, K. Torizuka, A. J. Manninen, J. M. Kyynäräinen, and G. E. Volovik, Phys. Rev. Lett. **65**, 3293 (1990).
- ¹⁴ P. J. Hakonen, O. T. Ikkala, and S. T. Islander, Phys. Rev. Lett. **49**, 1258 (1982).
- ¹⁵ H. K. Seppälä and G. E. Volovik, J. Low Temp. Phys. **51**, 279 (1983).
- ¹⁶ J. T. Simola, L. Skrbek, K. K. Nummilla, and J. S. Korhonen, Phys. Rev. Lett. **58**, 904 (1987).
- ¹⁷ Ü. Parts, E. V. Thuneberg, G. E. Volovik, J. H. Koivuniemi, V. M. H. Ruutu, M. Heinilä, J. M. Karimäki, and M. Krusius, Phys. Rev. Lett. **72**, 3839 (1994).
- ¹⁸ N. D. Mermin and T.-L. Ho, Phys. Rev. Lett. **36**, 594 (1976).
- ¹⁹ T. Ohmi, T. Tsuneto, and T. Fujita, Prog. Theor. Phys. **70**, 647 (1983).
- ²⁰ M. Fogelström and J. Kurkijärvi, J. Low Temp. Phys. **98**, 195 (1995); **100**, 597 (1995).
- ²¹ Ü. Parts, J. M. Karimäki, J. H. Koivuniemi, M. Krusius, V. M. H. Ruutu, E. V. Thuneberg, and G. E. Volovik, Phys. Rev. Lett. **75**, 3320 (1995).
- ²² J. M. Karimäki and E. V. Thuneberg, Phys. Rev. **B60**, 15290 (1999).
- ²³ N. Schopohl, J. Low Temp. Phys. **41**, 409 (1980).
- ²⁴ K. Scharnberg and R. A. Klemm, Phys. Rev. **B22**, 5233 (1980).
- ²⁵ T. Kita, Phys. Rev. Lett. **86**, 834 (2001).
- ²⁶ T. Kita, J. Phys. Soc. Jpn. **67**, 2067 (1998).
- ²⁷ T. Kita, J. Phys. Soc. Jpn. **67**, 2075 (1998).
- ²⁸ T. Kita, Phys. Rev. Lett. **83**, 1846 (1999).
- ²⁹ K. Yasui and T. Kita, Phys. Rev. Lett. **83**, 4168 (1999).
- ³⁰ T. Kita: Physica **B284-288**, 531 (2000).
- ³¹ J. W. Serene and D. Rainer, Phys. Rep. **101**, 221 (1983).
- ³² D. S. Greywall, Phys. Rev. **B33**, 7520 (1986).
- ³³ J. A. Sauls and J. W. Serene, Phys. Rev. **B24**, 183 (1981).
- ³⁴ E. V. Thuneberg, J. Low Temp. Phys. **122**, 657 (2001).
- ³⁵ J. C. Wheatley, Rev. Mod. Phys. **47**, 415 (1975).
- ³⁶ A. J. Leggett, Rev. Mod. Phys. **47**, 331 (1975).
- ³⁷ P. W. Anderson and W. F. Brinkman, in *The Physics of Liquid and Solid Helium* Part II, ed. by K. H. Bennemann and J. B. Ketterson (Wiley, New York, 1978) p. 177.
- ³⁸ See, e.g., M. Abramowitz and I. A. Stegun: *Handbook of Mathematical Functions* 10th ed. (Dover, New York, 1972).
- ³⁹ W. H. Press, S. A. Teukolsky, W. T. Vetterling and B. P. Flannery: *Numerical Recipes in C* (Cambridge University Press, Cambridge, 1988) Chap. 10.
- ⁴⁰ M. M. Doria, J. E. Gubernatis and D. Rainer: Phys. Rev. **B39** (1989) 9573.
- ⁴¹ *International Tables for Crystallography*, edited by Th. Hahn (Kluwer Academic Publishing, Dordrecht, 2002) Volume A.
- ⁴² C. J. Brandley and A. P. Cracknell, *The Mathematical Theory of Symmetry in Solids*, (Oxford University Press, Oxford, 1972).
- ⁴³ L. D. Landau and E. M. Lifshitz, *Statistical Physics Part 1*, (Pergamon, New York, 1980) §145.
- ⁴⁴ In the weak-coupling model of $-2\beta_1 = \beta_2 = \beta_3 = \beta_4 = -\beta_5$, the state $\tilde{A}_\mu^{(\pm 1)} \neq 0$ ($\mu = x$ or y) is degenerate with the state of Eq. (37).
- ⁴⁵ Any choice from $\mathbf{q}_2 - \mathbf{q}_1 = \pm \mathbf{b}_1/2$, $\pm \mathbf{b}_2/2$, and $(\pm \mathbf{b}_1 \pm \mathbf{b}_2)/2$ provides essentially an identical result.
- ⁴⁶ T.-L. Ho, Ph.D. thesis, Cornell University, 1978 (unpublished).